

# Transmission electron microscopy study of $\text{GdBa}_2\text{Cu}_3\text{O}_{7-x}$ containing nano-sized $\text{BaMO}_3$ (M: Hf, Zr, Sn) rods fabricated by pulsed laser deposition

D. Yokoe · T. Kato · H. Tobita · A. Ibi ·  
M. Yoshizumi · T. Izumi · T. Hirayama ·  
Y. Shiohara

Received: 2 April 2012 / Accepted: 14 September 2012 / Published online: 26 September 2012  
© Springer Science+Business Media New York 2012

**Abstract** Three types of superconducting  $\text{GdBa}_2\text{Cu}_3\text{O}_{7-x}$  (GdBCO) layers containing rods of either  $\text{BaHfO}_3$  (BHO),  $\text{BaZrO}_3$  (BZO), or  $\text{BaSnO}_3$  (BSO) were fabricated by pulsed laser deposition on Hastelloy substrates with a  $\text{CeO}_2$  based textured buffer layer. The critical currents ( $J_c$ ) values of the GdBCO layers containing those nano-rods are enhanced compared with those of pristine GdBCO layer in high magnetic fields. In order to investigate the relationships between their superconductive properties and their nanostructures, they were characterized in detail by transmission electron microscopy (TEM). TEM is the only method for direct observation of these nano-rods in the GdBCO grains. The GdBCO layers were mainly composed of  $c$ -axis oriented GdBCO grains containing numerous nano-sized rods. The crystal orientation relationships between the GdBCO and the nano-rods were as follows;  $(001)\text{GdBCO} // (001)\text{nano-rods}$  and  $(100)\text{GdBCO} // (100)\text{nano-rods}$ . The average diameters of the BHO and the BZO nano-rods were 4.5 and 5.6 nm, respectively. The BSO nano-rods were thicker than other rods. These nano-rods in the central region of the  $c$ -axis oriented GdBCO grains were aligned parallel to the  $c$ -axis of the GdBCO, while nano-rods in the outer region of the  $c$ -axis oriented grains were tilted away from the  $c$ -axis. With increase in the thickness of the GdBCO layers, the ratio of the BZO or

the BSO nano-rods aligned parallel to the  $c$ -axis to those tilted away from the  $c$ -axis decreased, so that the  $J_c$ - $B$ - $\theta$  profiles of the thicker GdBCO layers containing the BZO or the BSO nano-rods became flatter. The BHO nano-rods were homogeneously distributed throughout the GdBCO, and their average length of was less than that of the other nano-rods. The homogeneous distribution and short length of the BHO nano-rods enhanced the  $J_c$  values of the GdBCO layers containing them in high magnetic fields. The  $J_c$ - $B$ - $\theta$  profiles of the GdBCO layers containing the BHO were independent of the layer thickness. From these results, we will discuss about the morphologies and distributions of suitable vortex pinning for applications of GdBCO coated conductor in high magnetic fields.

## Introduction

The second-generation yttrium-based superconductive coated conductors with high critical current ( $I_c$ ) values have been developed. They can be as much as 0.5–1 km long, and their  $I_c$  values at 77 K and 0 T can be more than 500 A/cm. However, their  $I_c$  values still degrade in high magnetic fields and strongly depend on the angle applied magnetic fields, because of its anisotropic crystal structure and short coherence length. In order to develop superconductive instruments, such as superconducting magnetic energy storage (SMES), superconductive transformers, cables, and motors, using the coated conductors, it is necessary to enhance the  $I_c$  values of the coated conductors in high magnetic fields. This suggests the importance of formation of strong vortex pinning centers in the superconductive layer, so many researchers have tried to form high density defects or distribute nano-sized particles [1–12] to act as the pinning centers in the superconductive

D. Yokoe · T. Kato (✉) · T. Hirayama  
Nanostructures Research Laboratory, Japan Fine Ceramics  
Center, 2-4-1 Mutsumo Atsuta-ku, Nagoya 456-8587, Japan  
e-mail: tkato@jfcc.or.jp

H. Tobita · A. Ibi · M. Yoshizumi · T. Izumi · Y. Shiohara  
Superconductivity Research Laboratory, International  
Superconductivity Technology Center, 1-10-13 Shinonome,  
Koto-ku, Tokyo 135-0062, Japan

layer. In particular, nano-sized rods perpendicular to the substrate can be formed in superconductive layers fabricated by pulsed laser deposition (PLD) [1, 3–10]. The  $J_c$  values of such superconductive layers increase more under a high magnetic field perpendicular to the substrate than those of superconductive layers without such nano-rods [4, 5]. In addition, it was confirmed that the field angle dependence of  $\text{GdBa}_2\text{Cu}_3\text{O}_{7-x}$  (GdBCO) layers containing the nano-rods fabricated by PLD could be reduced and the  $J_c$  values of the GdBCO enhanced in high magnetic fields compared with those of  $\text{YBa}_2\text{Cu}_3\text{O}_{7-x}$  containing the nano-rods [5].

In this study, three types of GdBCO layers containing nano-rods of either  $\text{BaHfO}_3$  (BHO),  $\text{BaZrO}_3$  (BZO), or  $\text{BaSnO}_3$  (BSO) were fabricated by PLD on Hastelloy substrate with a  $\text{CeO}_2$  based textured buffer layer. We characterized the nanostructures of these GdBCO layers in detail using transmission electron microscopy (TEM). In particular, to clarify the relationships between the superconductive properties and the nanostructures of the GdBCO layers containing the nano-rods, the orientations, sizes, and distribution of the rods were examined using selected area diffraction pattern and moiré fringes.

## Experimental procedure

The three types of sintered materials used as target materials were synthesized, in which either 3.5 mol% BHO, 5.0 mol% BZO, or 7.5 mol% BSO particles had been added to the GdBCO matrix, which were the particle contents yielding GdBCO layer with the highest critical current density ( $J_c$ ) values at 77 K and a magnetic field of 3 T [13]. Hastelloy tapes with a textured  $\text{CeO}_2/\text{LaMnO}_3/\text{MgO}/\text{Gd-Zr-O}$  layer were transmitted during the PLD process using reel-to-reel transfer system [14]. In order to investigate the thickness dependence of the  $J_c$  in high magnetic fields, we prepared 1  $\mu\text{m}$ -thick and more than 2.5  $\mu\text{m}$ -thick GdBCO layers containing each nano-rods.

These GdBCO layers were thinned at Ga-ion accelerating voltage ranging from 1 to 40 kV in a Hitachi NB5000 focused ion beam-scanning electron microscopy dual-beam system equipped with a micro-sampling system to prepare cross-sectional and plan-view TEM specimens. In the plan-view specimen, the membranes from the surface region of the GdBCO layers to the  $\text{CeO}_2$  interface were prepared so that the GdBCO layers could be observed continuously, as shown in Fig. 1 [15]. The specimens were examined in a TOPCON EM-002B and EM-002BF TEM at an accelerating voltage of 200 kV. Energy dispersive X-ray spectroscopy (EDS) elemental maps were acquired by a Noran System Seven with twin EDS detectors in the TOPCON EM002BF.

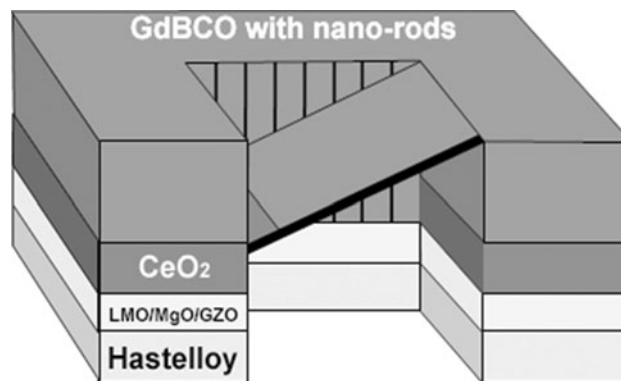


**Fig. 1** Schematic illustration of a plan-view specimen of GdBCO layer containing nano-rods on Hastelloy with a textured  $\text{CeO}_2/\text{LaMnO}_3(\text{LMO})/\text{MgO}/\text{Gd-Zr-O}(\text{GZO})$

## Results and discussion

Figure 2 shows the field angle dependence of  $J_c$  of the GdBCO layers containing (a) 3.5 mol% BHO, (b) 5.0 mol% BZO, and (c) 7.5 mol% BSO nano-rods at 77 K under a magnetic field of 3 T [13], where the open symbols correspond to 1  $\mu\text{m}$ -thick GdBCO layers and the solid symbols to more than 2.5  $\mu\text{m}$ -thick. The  $J_c$ - $B$ - $\theta$  profiles of both the thin and the thick layer with BHO nano-rods are almost the same, whereas the  $J_c$ - $B$ - $\theta$  profiles of the thicker layers with BZO or BSO are both lower and flatter. It is well known that the  $J_c$  values of yttrium-based superconductive layers decrease with increasing layer thickness. In the case of GdBCO layers fabricated by PLD, outer growth grains, which are misaligned GdBCO crystals compared with matrix  $c$ -axis oriented GdBCO grains, are formed in the layers [16]. In addition, since the outer growth GdBCO grains prevent superconductor current, grain growth of the grains is one of the reasons for the  $J_c$  reduction [16]. Numerous outer growth grains were formed in all GdBCO layers, so that the  $J_c$  reductions of the thicker GdBCO layers containing the BZO or the BSO nano-rods occurred at 77 K and a magnetic field of 3T. In contrast, the  $J_c$  reduction of the thicker GdBCO layer containing BHO nano-rods is quite low at 77 K and a magnetic field of 3 T, in spite of the formation of the outer growth grains, as shown in Fig. 2a.

Figure 3 shows low magnification cross-sectional electron micrographs of the thicker GdBCO layers containing (a) 3.5 mol% BHO, (b) 5.0 mol% BZO, and (c) 7.5 mol% BSO nano-rods on a  $\text{CeO}_2$  buffer layer under the  $\bar{g} = 006$  of GdBCO condition. The thicknesses of the GdBCO containing the BHO, the BZO, and the BSO nano-rods are 2.9, 2.8, and 2.6  $\mu\text{m}$ , respectively. These GdBCO layers are mainly composed of  $c$ -axis oriented GdBCO grains. In this condition, screw dislocations in the  $c$ -axis oriented GdBCO grains were found to appear as thick dark lines perpendicular to the substrate [15]. Multilayered GdBCO structures along

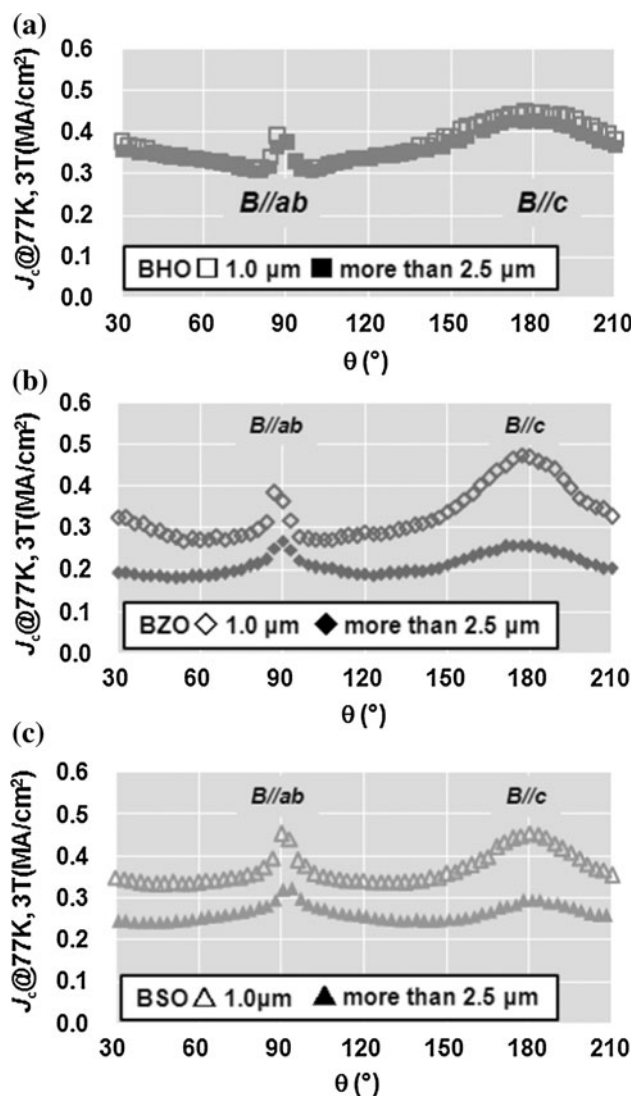


**Fig. 2** Field angle dependence of  $J_c$  of a GdBCO layers containing a 3.5 mol% BHO, b 5.0 mol% BZO, and c 7.5 mol% BSO nano-rod at 77 K under a magnetic field of 3 T. *Open symbols* correspond to 1  $\mu\text{m}$ -thick GdBCO layers and *solid symbols* to more than 2.5  $\mu\text{m}$ -thick

the interface between the GdBCO and the  $\text{CeO}_2$  are seen in Fig 2a–c. These boundaries, indicated by arrows, correspond to the multiple PLD deposition using the reel-to-reel tape transfer system to fabricate the thicker GdBCO layer.

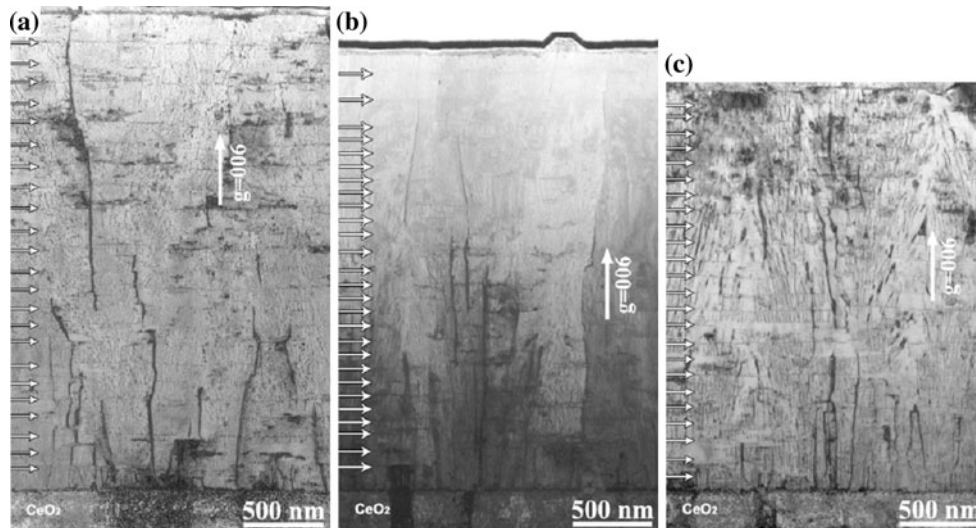
Figure 4 shows selected area diffraction patterns from the GdBCO layers containing (a) 3.5 mol% BHO, (b) 5.0 mol% BZO, and (c) 7.5 mol% BSO and plane indexes. The nano-rod are coherent to the matrix GdBCO grains. According to the diffraction patterns in Fig. 3, the crystal orientation relationships between the GdBCO and the nano-rod are as follows:  $(001)\text{GdBCO} // (001)\text{nano-rod}$  and  $(100)\text{GdBCO} // (100)\text{nano-rod}$ .

Figure 5 shows higher magnified cross-sectional TEM images of (a) the BHO, (b) the BZO, and (c) the BSO

nano-rods in the GdBCO layers under the  $\bar{g} = 006$  of GdBCO condition. These nano-rods in GdBCO layers appear as moiré fringes because of the orientation relationships between the nano-rods and the GdBCO described above [7]. The relationships between spacing ( $D$ ) of moiré fringes and lattice spacing ( $d_1, d_2$ ) is written as follows:  $D = [d_1 d_2 / |d_1 - d_2|] \cos\theta$ . Here,  $\cos\theta$  is 1 because of the cube on cube crystal orientation relationship mentioned above. The moiré fringes  $D$  spacing, shown in Fig. 5a–c, were measured as 2.9, 2.8, and 3.6 nm, respectively. Since Fig. 5a–c are taken under the  $\bar{g} = 006$  of GdBCO condition, these  $D$  values would be caused by  $d_1$  of the  $(006)\text{GdBCO}$  plane of 0.1949 nm and  $d_2$  of the  $(002)\text{nano-rod}$  plane of 0.2085 nm (BHO), 0.2091 nm (BZO), or 0.2058 nm (BSO), respectively.

According to this cross-sectional observation shown in Fig. 5, the average diameters of the BHO, the BZO, and the BSO nano-rods are 4.5, 5.6, and 9.4 nm, respectively. Figure 6 shows EDS elemental maps of (a) Hf of the BHO nano-rods, (b) Zr of the BZO nano-rods and (c) Sn of the BSO nano-rods in GdBCO, and (d–f) TEM image of the corresponding region of (a–c), respectively. These nano-rods formed along the substrate normal. These cross-sectional observations confirm that the BHO nano-rods are thinner and shorter than the other nano-rods.

A low magnification plan-view image of the 2.9  $\mu\text{m}$ -thick GdBCO layer containing the BHO nano-rods is shown in Fig. 7; where the entire GdBCO layer from the  $\text{CeO}_2$  interface, indicated by a straight broken line, to surface region can be observed. Left hand side corresponds to the  $\text{CeO}_2$  interface side and the opposite side to the surface region of the GdBCO layer in Fig. 7. Since incident electron beam is along the  $\langle 001 \rangle$  of the  $c$ -axis oriented GdBCO grains in Fig. 7, twin boundaries along  $\{110\}$  are found in the  $c$ -axis oriented GdBCO grains as shown in Fig. 7 [15]. Some outer growth GdBCO grains indicated by arrows in Fig. 7 have different orientation compared with that of the matrix  $c$ -axis oriented GdBCO grains; nevertheless, BHO nano-rods form in such outer growth grains surrounded by a broken line, as shown in Fig. 8. Figure 9a–c show higher magnification plan-view images of the regions labeled A–C in Fig. 7. In order to emphasize the BHO nano-rods, plan-view specimen was slightly tilted along the  $\langle 100 \rangle$  of the  $c$ -axis oriented GdBCO grains in Fig. 9a–c. White lines indicate the grain boundaries of the  $c$ -axis oriented grains in Fig. 9. The GdBCO grains grow larger with increasing thickness of the GdBCO layer. The BHO nano-rods are seen as dots in the central part of the  $c$ -axis oriented grains. In other words, BHO nano-rods in that part are clearly aligned in the  $c$ -axis of the GdBCO grains. On the contrary, the nano-rods in the region around the grain boundaries are observed as linear shape. In other words, BHO nano-rods in



**Fig. 3** Low magnification cross-sectional electron micrographs of thicker GdBCO layers containing **a** 3.5 mol% BHO, **b** 5.0 mol% BZO, and **c** 7.5 mol% BSO nano-rods on a  $\text{CeO}_2$  buffer layer under the  $\bar{g} = 006$  of GdBCO condition

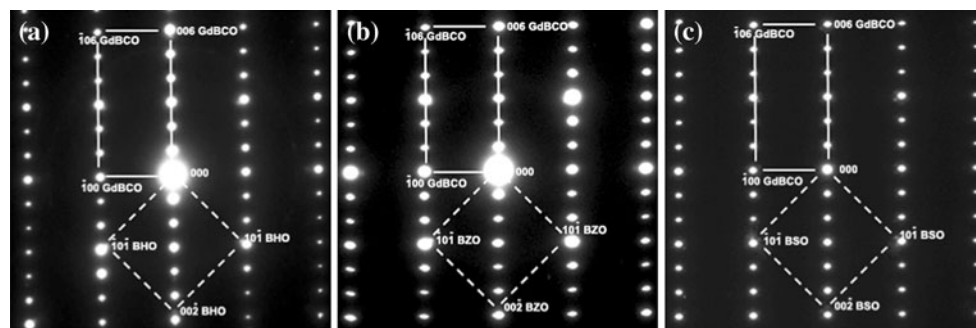


**Fig. 4** Selected area diffraction patterns from GdBCO layers containing **a** 3.5 mol% BHO, **b** 5.0 mol% BZO, and **c** 7.5 mol% BSO and plane indexes

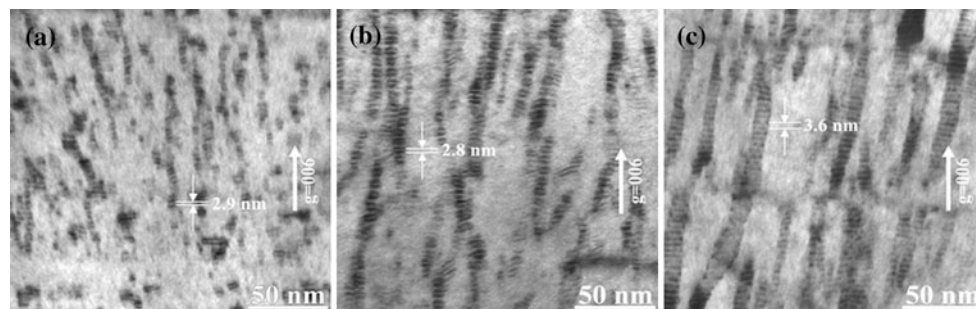


**Fig. 5** Cross-sectional TEM images of **a** BHO, **b** BZO, and **c** BSO nano-rods in GdBCO layers under the  $\bar{g} = 006$  of GdBCO condition

outer region of the  $c$ -axis oriented grains are tilted away from the  $c$ -axis. However, the dots contrast in the central part and linear shape contrast in the outer region of the GdBCO grains are similar from the vicinity of the  $\text{CeO}_2$  region to the surface region, due to the shorter length of the BHO nano-rods, as shown in Fig. 9a–c. Therefore, there is no significant difference of the distribution and the densities of the BHO nano-rods in the GdBCO grains from the  $\text{CeO}_2$  interface to

the surface region. Using this plan-view observation, inner and outer of GdBCO grains can be observed at the same time. Therefore, the orientation and the distribution of the nano-rods in the grains can accurately be recognized compared to the cross-sectional observation.

Plan-view specimens of a 2.8  $\mu\text{m}$ -thick GdBCO layer containing the BZO nano-rods and a 2.6  $\mu\text{m}$ -thick GdBCO with BZO nano-rods were prepared using the same procedure.

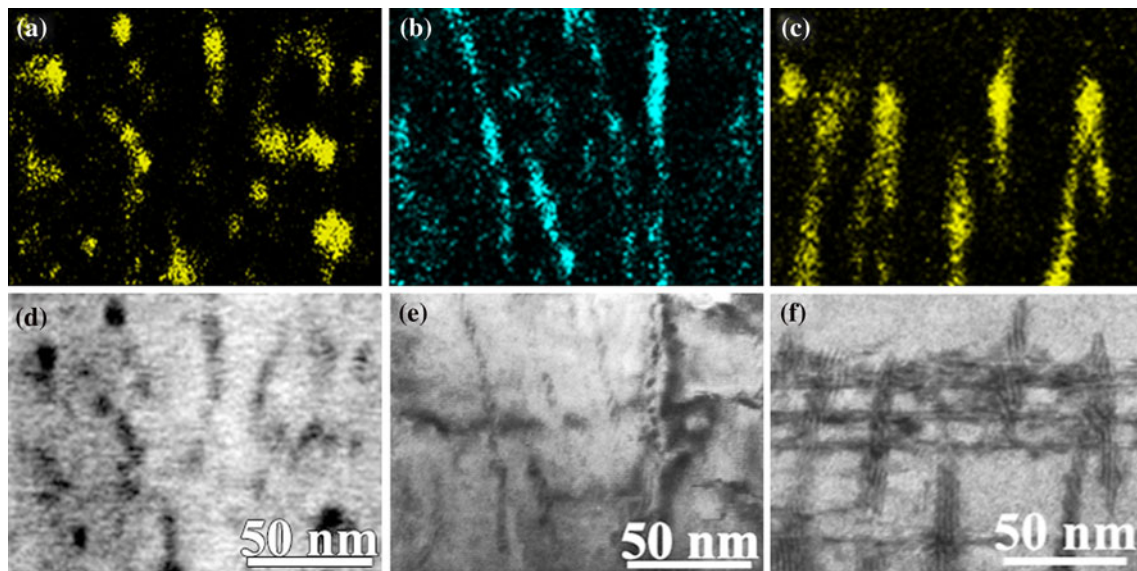


**Fig. 6** EDS elemental maps of **a** Hf of BHO nano-rods, **b** Zr of BZO, and **c** Sn of BZO in GdBCO. **d–f** Corresponding BF images to regions (**a–c**), respectively



**Fig. 7** Low magnification plan-view image of 2.9  $\mu\text{m}$ -thick GdBCO layer containing BHO nano-rods. *Left hand side* corresponds to  $\text{CeO}_2$  interface side and the *opposite side* to surface region

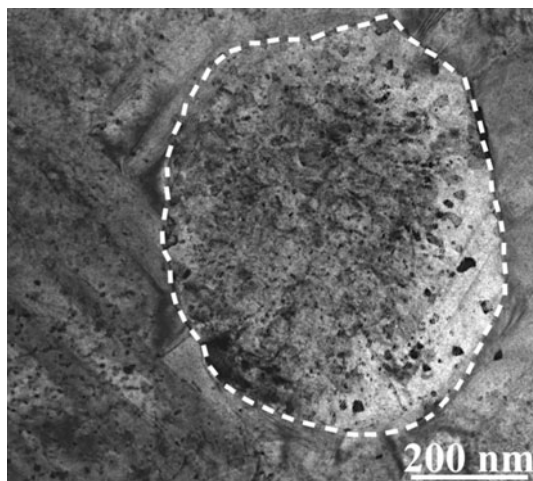


**Fig. 8** Plan-view image of an outer growth GdBCO grain with BHO nano-rods

Figure 10 shows plan-view images of the GdBCO layers containing (a) the BZO nano-rods and (b) the BSO nano-rods near the  $\text{CeO}_2$  interface, and grain boundaries of  $c$ -axis oriented grains are indicated by white lines. Both kinds of the

nano-rods appear as dots so that they are aligned in the  $c$ -axis of the GdBCO grains. Figure 11 shows plan-view images of the surface regions of the GdBCO layers containing (a) the BZO rods and (b) the BSO rods, and white lines indicate the grain boundaries of  $c$ -axis oriented grains. The GdBCO grains, containing the BZO or the BZO nano-rods, grew larger with increasing GdBCO layer thickness as well as the GdBCO layer with the BHO. In the central region of  $c$ -axis oriented GdBCO grain, both the BZO and the BSO nano-rods are seen as dots, while these rods are observed as longer linear contrast in the outer region of the same GdBCO grains, compared to the BHO nano-rods as shown in Fig. 9. Therefore, the BZO and the BSO nano-rods are aligned in the  $c$ -axis of the GdBCO grains in the central part, though these nano-rods are tilted away from the  $c$ -axis in the outer region of the same GdBCO grain. Since the BZO and the BSO nano-rods are longer than that of BHO, fire-works structures [8–10] of the BZO and the BSO nano-rods is more prominent than those of the BHO nano-rods. In addition, thick BSO nano-rods with more than 20 nm in diameter, which has not been observed in the cross-sectional specimen, are seen in the surface region of the GdBCO layer as shown in Fig. 11b.

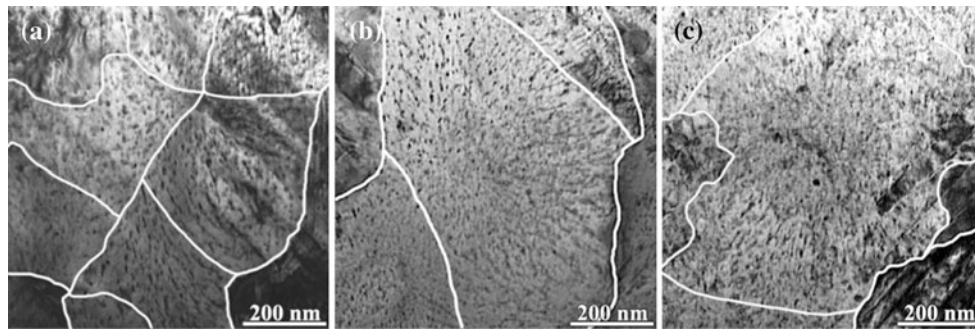


**Fig. 9** Plan-view images of GdBCO containing BHO nano-rods. **a–c** Corresponds the region of A–C in Fig. 7. *White lines* indicate grain boundaries of *c*-axis oriented grains

**Fig. 10** Plan-view images of GdBCO layers containing **a** BZO nano-rods and **b** BSO nano-rods near the  $\text{CeO}_2$  interface

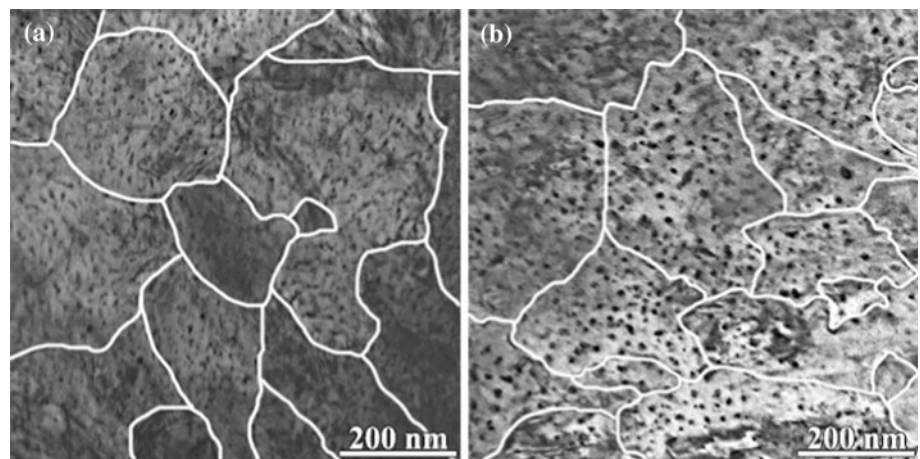
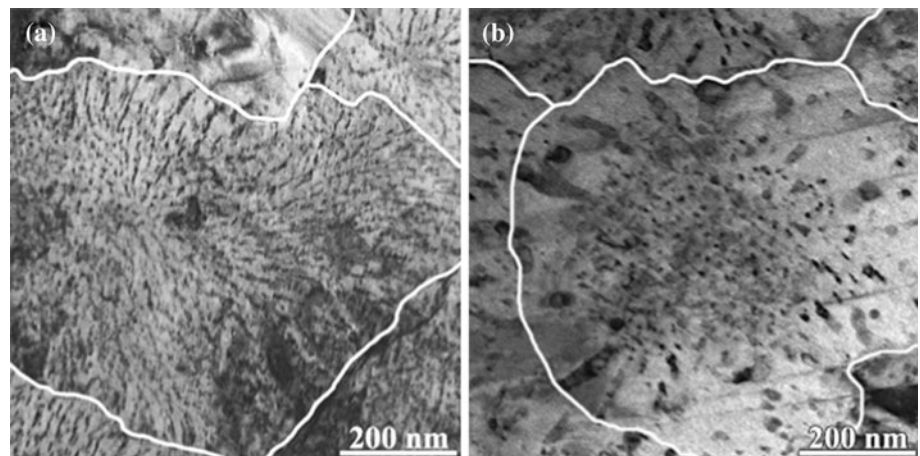


**Fig. 11** Plan-view images of surface regions of the GdBCO layers containing **a** BZO nano-rods and **b** BSO nano-rods. *Broken lines* indicate grain boundaries of *c*-axis oriented grains



These plan-view observations indicate that the ratio of the BZO and the BSO nano-rods aligned in the *c*-axis of the GdBCO grains, which act as *c*-axis correlated pinning centers, to those tilted away from the *c*-axis decreases with increasing thickness of the GdBCO layers. As a result, the  $J_c$ - $B$ - $\theta$  profiles of GdBCO layer containing the BZO or the

BZO nano-rods become flatter in thicker layers due to reduction of the peak around magnetic field angle of  $180^\circ$  ( $B//c$ ), as shown in Fig. 2b, c. In contrast, the BHO nano-rods are homogeneously distributed throughout the GdBCO layer and are shorter than the BZO and the BSO nano-rods. These distributions, orientations, and short length of the BHO

nano-rods should be strongly correlated with the  $J_c$ - $B$ - $\theta$  profiles at 77 K and a magnetic field of 3 T, as shown in Fig. 2a.

High density and homogeneous distribution of nano-sized non-superconductive particles in the GdBCO layer is the ideal state for vortex pinning centers in high magnetic fields. In addition, small volume percentage of the particles in the layers should be better such that it does not decrease the superconductor current. Since these particles can trap high dense vortex applying from all magnetic fields angles, it is possible to reduce field angular dependence of  $J_c$  values of the GdBCO layers. For these reasons, both the short length and the small diameter of the BHO nano-rods is better morphology for the vortex pinning center, and the small amount of the addition (3.5 mol%) has advantage compared with those of the BZO (5.0 mol%) and BSO (7.5 mol%) nano-rods.

## Summary

Three types of GdBCO layers containing nano-sized rods of either BHO, BZO, or BSO were deposited by PLD on Hastelloy substrates with a textured  $\text{CeO}_2/\text{LaMnO}_3/\text{MgO}/\text{Gd-Zr-O}$  buffer layer. The nanostructures of these GdBCO layers containing each nano-rods were characterized in detail by TEM. The GdBCO layers were mainly composed of  $c$ -axis oriented GdBCO grains containing numerous nano-sized BHO, BZO, or BSO rods. Selected area diffraction patterns revealed that the crystal orientation relationships between the GdBCO and the nano-rods were (001)GdBCO// (001)nano-rods and (100)GdBCO//(100)nano-rods. The average diameters of the BHO and the BZO were 4.5 and 5.6 nm, respectively. The BSO nano-rods were thicker than other rods. These nano-rods in the central region of the  $c$ -axis oriented GdBCO grains were aligned in the  $c$ -axis of the GdBCO, while the nano-rods in the outer region of the  $c$ -axis oriented grains were tilted away from its  $c$ -axis. With increasing thickness of the GdBCO layers, the ratio of the BZO or the BSO nano-rods aligned in the  $c$ -axis of the GdBCO grains to those tilted away from the  $c$ -axis reduced, so that the  $J_c$ - $B$ - $\theta$  profiles of the thicker GdBCO layers containing the BZO or the BZO nano-rods became flatter at 77 K and a magnetic field of 3 T. The average length of the BHO nano-rods was shorter than that of the other rods and they were homogeneously distributed throughout the GdBCO layer. Therefore, the  $J_c$ - $B$ - $\theta$  profiles of the GdBCO

layers containing the BHO nano-rods do not depend on the layer thickness at 77 K and a magnetic field of 3 T.

**Acknowledgements** This work was supported by New Energy and Industrial Technology Development Organization (NEDO) as the project for Development of Materials & Power Applications of Coated Conductors.

## References

1. Driscoll JLM, Foltyn SR, Jia QX, Wang H, Serquis A, Civale L, Maiorov B, Hawley M, Maley MP, Peterson DE (2004) *Nat Mater* 3:439–441
2. Haugan T, Barnes PN, Wheeler R, Meisenkothen F, Sumption M (2004) *Nature* 430:867–870
3. Matsumoto K, Horide T, Ichinose A, Horii S, Yoshida Y, Mukaida M (2005) *Jpn J Appl Phys* 44:L246–L248
4. Yamada Y, Takahashi K, Kobayashi H, Konishi M, Watanabe T, Ibi A, Muroga T, Miyata S, Kato T, Hirayama T, Shiohara Y (2005) Pinning effective nano-epitaxial columnar structure and defect in  $\text{Y}(\text{RE})\text{Ba}_2\text{Cu}_3\text{O}_{7-x}$  coated conductor. *Appl Phys Lett* 87:132502
5. Takahashi K, Kobayashi H, Yamada Y, Ibi A, Fukushima H, Kobayashi M, Miyata S, Shiohara Y, Kato T, Hirayama T (2006) *Supercond Sci Technol* 19:924–929
6. Kato T, Sasaki H, Gotoh Y, Sasaki Y, Hirayama T, Takahashi K, Konishi M, Kobayashi H, Ibi A, Muroga T, Miyata S, Watanabe T, Yamada Y, Izumi T, Shiohara Y (2006) *Physica C* 445–448: 628–632
7. Yamada K, Ichinose A, Tomokiyo Y, Shingai Y, Matsumoto K, Yoshida Y, Horii S, Kita R, Toh S, Kaneko K, Mori N, Mukaida M (2007) *Jpn J Appl Phys* 46(2):708–711
8. Ichinose A, Mele P, Horide T, Matsumoto K, Goto G, Mukaida M, Kita R, Yoshida Y, Horii S (2008) *Physica C* 468:1627–1630
9. Mele P, Matsumoto K, Horide T, Ichinose A, Mukaida M, Yoshida Y, Horii S, Kita R (2008) *Supercond Sci Technol* 21: 032002
10. Kaneko K, Furuya K, Yamada K, Sadayama S, Barnard JS, Midgley PA, Kato T, Hirayama T, Kiuchi M, Matsushita T, Ibi A, Yamada Y, Izumi T, Shiohara Y (2010) *J Appl Phys* 108:063901
11. Gutiérrez J, Llordés A, Gázquez J, Gibert M, Romà N, Ricart S, Pomar A, Sandiumenge F, Mestres N, Puig T, Obradors X (2007) *Nat Mater* 6:367–373
12. Miura M, Kato T, Yoshizumi M, Yamada Y, Izumi T, Shiohara Y, Hirayama T (2008) *Appl Phys Exp* 1:051701
13. Tobita H, Notoh K, Higashikawa K, Inoue M, Kiss T, Kato T, Hirayama T, Yoshizumi M, Izumi T, Shiohara Y (2012) *Supercond Sci Technol* 25:062002
14. Ibi A, Iwai H, Takahashi K, Muroga T, Miyata S, Watanabe T, Yamada Y, Shiohara Y (2005) *Physica C* 426–431:910–914
15. Kato T, Sasaki H, Watanabe T, Ibi A, Iwai H, Iijima Y, Kakimoto K, Sutoh Y, Muroga T, Miyata S, Yamada Y, Saitoh T, Izumi T, Sasaki Y, Hirayama T, Shiohara Y, Ikuhara Y (2006) *J Mater Sci* 41:2587. doi:10.1007/s10853-006-7785-2
16. Kato T, Yoshida R, Chikumoto N, Lee S, Tanabe K, Izumi T, Hirayama T, Shiohara Y (2011) *Physica C* 471:1012–1016